NOTES AND CORRESPONDENCE

A Spatial Two-Dimensional Discrete Filter for Limited-Area-Model Evaluation Purposes

FRAUKE FESER AND HANS VON STORCH

Institute for Coastal Research, GKSS Research Centre, Geesthacht, Germany

(Manuscript received 24 September 2004, in final form 12 November 2004)

ABSTRACT

A two-dimensional discrete spatial filter was developed. It serves as a means to classify meteorological fields on a limited-area grid according to their spatial dimensions by filtering certain wavenumber ranges. Thereby it performs an isotropic spatial-scale separation of the atmospheric fields. A general algorithm was developed, which allows the construction of a filter that closely approximates a specific isotropic response function. The filter is simple in the construction and easy to apply while giving reasonable results. The method allows for considerable flexibility in choosing this specific response. This way, low-, band-, and high-pass filters are obtained. Examples show an effective scale separation of atmospheric fields on limited-area grids that can be used for process studies, model evaluation, or comparisons.

1. Introduction

Limited-area models (LAMs) for the atmosphere are used for simulating the regional climate (Giorgi et al. 2001). The spatial gridding of these regional climate models (RCMs) currently ranges from about 50 to 10 km, and time periods of up to several decades have been simulated. However, the question if RCMs provide added value compared to global analyses [such as the National Centers for Environmental Prediction (NCEP)–National Center for Atmospheric Research (NCAR) reanalysis; Kalnay et al. 1996] or global models of lower resolution is still only partly answered. We believe this is mainly due to the lack of a convenient tool to properly describe the added value—namely, a filter procedure that compares the performance of the global analysis or model with that of the regional model on large and medium-to-small spatial scales. In this paper, we suggest using digital filters for the separation of components of a limited spatial field with different spatial scales. The spatially filtered fields may then be used for model validation, diagnostic purposes, or comparisons between the global coarse-grid data and the regional model refinement.

When identifying the added value of RCM simulations, we suggest the application of the downscaling paradigm that states that smaller-scale dynamics may be understood as being conditioned by large-scale variability and physiographic regional detail (von Storch 1995). In doing so, we consider the large scales described properly by the global analyses or global climate models. On the other hand, the global models and analyses have little skill at scales smaller than a few grid points, for example, a few hundred kilometers. On these scales, we expect the added value of RCMs. In the present paper, we deal with the problem of how to achieve conveniently and efficiently this scale separation.

Spatial filters are rarely used for the evaluation of RCM output, in particular not in the context of regional climate simulations with an RCM. One approach, used in LAM forecasting and evaluation, is to expand a limited field in a 2D Fourier series, and to rebuild a filtered field by recombining only Fourier components with relevant scales (Errico 1985; Stamus et al. 1992). This Fourier concept was also incorporated into the spectral nudging or large-scale forcing concept by Waldron et al. (1996), von Storch et al. (2000), and Miguez-Macho et al. (2004), which keeps the large-scale part of a regional model solution close to the forcing global field in the model interior. Bettge and Baumhefner (1980) introduced digital filters using classical ideas proposed by Shuman (1957) and Shapiro (1970).

In the present paper, we provide an algorithm to

Corresponding author address: Frauke Feser, Institute for Coastal Research, GKSS Research Centre, P.O. Box, 21502 Geesthacht, Germany.
E-mail: feser@gkss.de

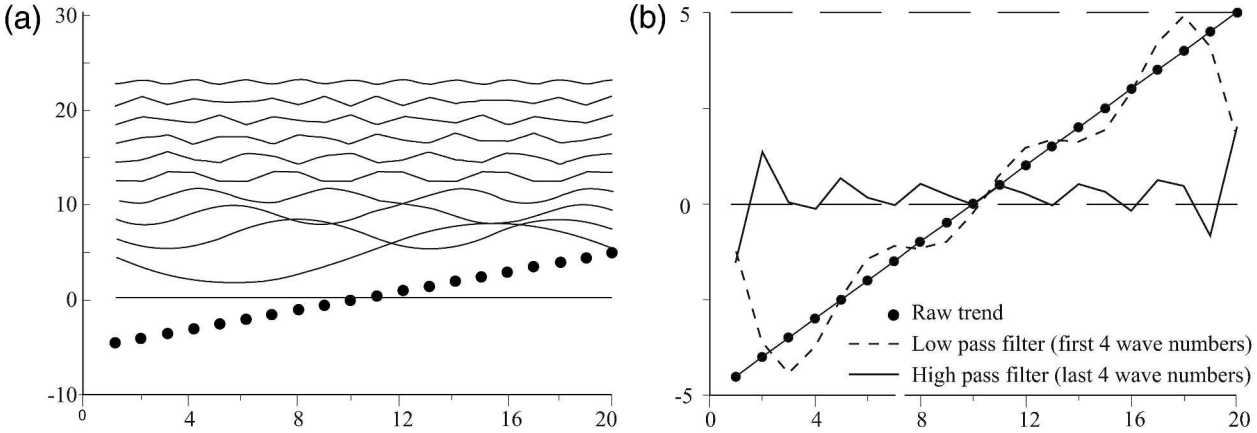

FIG. 1. Fourier decomposition of (a) a spatial trend and (b) a low- and high-pass Fourier-filtered spatial trend. The x axis denotes the grid points of the LAM.

construct two-dimensional digital filters for the spatial-scale separation of limited-area fields (sections 5 and 6). Examples of such filters are presented and their utility is demonstrated (section 7). Before doing so, we want to discuss alternatives to our approach.

The most straightforward approach is Errico's approach to decompose the two-dimensional field into a series of sinusoidal harmonics in x and y directions, as mentioned above. This approach has the distinctive advantage that the scale separation is very accurate. However, the harmonic analysis suffers from the erroneous description of spatial "trends" (nonsinusoidal components of the spatial fields, such as linear or higher polynomials) as being composed of "waves." The harmonic analysis works fine if the considered field is periodic. However, LAM output is almost never periodic and often exhibits a trend; for instance, in winter, air pressure is often lower over the ocean and higher over land. We demonstrate the problem of subjecting a "trend" to harmonic analysis by a synthetic example of a pure spatial trend without any wave components (Fig. 1a). This linear trend (shown as dots) can be decomposed into sine and cosine waves as shown in Fig. 1a. If this spatial trend is filtered with a Fourier low-pass filter (lowest four wave contributions of Fig. 1a were retained in this example), the resulting curve (dashed curve in Fig. 1b) replicates the overall trend but adds significant large-scale wave components—in particular at the margins. One might argue that in LAM applications the overshooting in the marginal zone would not matter, since it would affect only the sponge zone, which is normally not considered. However, there is also a false identification of short-wave contributions by the high-pass spatial filter (solid curve in Fig. 1b; shortest four wave contributions of Fig. 1a were retained), which is not limited to the sponge zone but which occurs also in the interior. The discrete cosine-filter method suggested by Denis et al. (2002) is better in describing spatial trends, but it also maps all variability on wavy components, so that any recombination of a subset of these components, which is needed for formulating a filter, may generate artificial wavy contributions.

Errico (1985) had noticed the problem of spatial trends and has suggested subtracting linear functions; in the following we extend his approach by considering not only linear but also quadratic polynomials (section 2).

Digital filters (e.g., Shuman 1957; Shapiro 1970, 1975) have the advantage that they operate with a finite "support base"; for example, the filtered value at some location is a function of the values in a neighborhood of that location and not, as in case of harmonic analysis, of all locations. The disadvantage is that the scale separation is less effective than with a Fourier filter, since the response function of a digital filter is smooth and not a step function as in the case of a Fourier filter. That is, for a low-pass filter, the long waves will not exactly be retained but only approximately; similarly, a high-pass filter will not completely remove all contributions of long waves—which is a problem, when the intensity of short waves is much smaller than those of long waves. Digital filters usually lead to a loss of data at the margins of the domain, as the determination of a filtered value needs data in a symmetric neighborhood of that point. However, with RCMs this is not a problem, as such models are run with a sponge zone within which little added value is expected. Thus, if the filtering neighborhood is not wider than the sponge zone, a scale separation for the entire relevant interior domain can be achieved.

Usually, digital filters are one-dimensional, and are applied to two-dimensional fields by first applying it in

one direction and then in the other. Bettge and Baumhefner (1980) used such a one-dimensional digital bandpass filter for obtaining a scale separation of limited-area atmospheric fields. They applied the 1–2–1 low-pass-filter operator presented by Shuman (1957) and created bandpass filters by repetition and differences. Another one-dimensional digital filter, namely a high-order, high-pass implicit filter, was used by Raymond (1989). Such filters are, unfortunately, not isotropic and their filter characteristics are not really flexible. Therefore a method for the flexible construction of a two-dimensional isotropic discrete filter was required. The filter weights are obtained by solving an approximation problem.

Two-dimensional wavelets (e.g., Yano et al. 2001; Desrochers and Yee 1999; Jameson et al. 2002) may be a promising, alternative approach. However, so far their application in scale separation used in regional climate modeling is very limited. For our limited-area model application with terabytes of data a fast filtering approach is essential. In general the image decomposition in fast wavelet algorithms is made with a dyadic resolution factor (Daubechies 1992; Starck et al. 1998). If, as in our case, special wavenumbers are of interest as cutoff frequencies they usually are not matched directly by the dyadic resolution approach. To achieve the separation into certain wavenumber bands a postprocessing of the wavelet with the multiresolution analysis (Mallat 1989, 1998) is necessary, which costs extra computing time, both in terms of determining the wavelet transform and the back transformation. We suggest that wavelets are not a viable alternative to our digital filters, which are computationally simple and adapted to the specific wavenumber band.

2. Preprocessing: Subtraction of two-dimensional polynomials

Before filtering, the meteorological fields in our study were "preprocessed," whereby two-dimensional polynomials were subtracted. This serves two purposes:

- Fourier expansions of fields on regionally limited grids suffer from the fact that the nonperiodic components are falsely represented by "waves." By identifying the dominant nonperiodic components P, we may conceptually express the 2D LAM fields as

$$f(x, y) = P_f^K(x, y) + L_f(x, y) + M_f(x, y) + S_f(x, y). \quad (1)$$

  Here, P_f^K represents the polynomial of kth order of the two-dimensional field f, L_f its large-scale wave component, M_f the medium-scale wave component, and S_f the short-scale wave component of f.

  When the P_f component is disregarded, the nonperiodic contribution falsely compounds the wavy components on all scales. Thus, the inclusion of P_f^K leads to a better separation and description of components.
- Practically, the separation into the three wave components L, M, and S is obtained by a digital filter. Such filters operate fine if the variance of the wavenumbers to be suppressed is not much larger than the variance that is supposed to be retained. This is always the case with low-pass filters, when high wavenumber variance is eliminated—high wavenumbers always have smaller variance than low wavenumbers. There is also not usually a problem for medium-pass filters. However, high-pass filters are usually negatively impacted, as the elimination of low-pass components is not perfect and minor remnants of low-wavenumber variability remain—and minor remnants are comparable to high-wavenumber contributions in terms of variance. An example for this is given in Errico (1987). The subtraction of polynomials can help to ease this problem, as this operation reduces the variance of the large scale.

Equations for the polynomial subtraction are given in appendix A. Figure 2 shows the $K = 1$ and $K = 2$ polynomials fitted to the wind speed on 3 December 1999, 6 p.m., and the total wind speed field as well as after subtraction of the $K = 1, 2$ polynomials. In contrast to the linear $K = 1$ polynomial, the fitted quadratic polynomial exhibits a marked nonlinear pattern, describing higher wind speeds over the North Atlantic and a gradual increase toward southern latitudes and continental areas. The wind speed field in the bottom of Fig. 2 is rather noisy. Thus the subtraction of the polynomials is not changing the overall character of the spatial wind speed distribution, but the NW–SE asymmetry is eliminated. We suggest subtracting the quadratic polynomials for data to be band- or high-pass filtered. The polynomial subtraction was applied to all band- and high-pass-filtered fields shown in section 7.

3. Selection of prespecified wavenumbers

The idea was to construct an almost isotropic filter. Thus, it is meaningful to select all wavenumbers with the same or similar two-dimensional wavenumber $k^* = \sqrt{k^2 + l^2}$ and to assign the same response $\kappa(k^*)$.

A low-pass filter is generated by requesting $\kappa(k^*) = 1$ for all k^* below a small wavenumber—for instance, 5—and $\kappa(k^*) = 0$ for all wavenumbers k^* larger than a

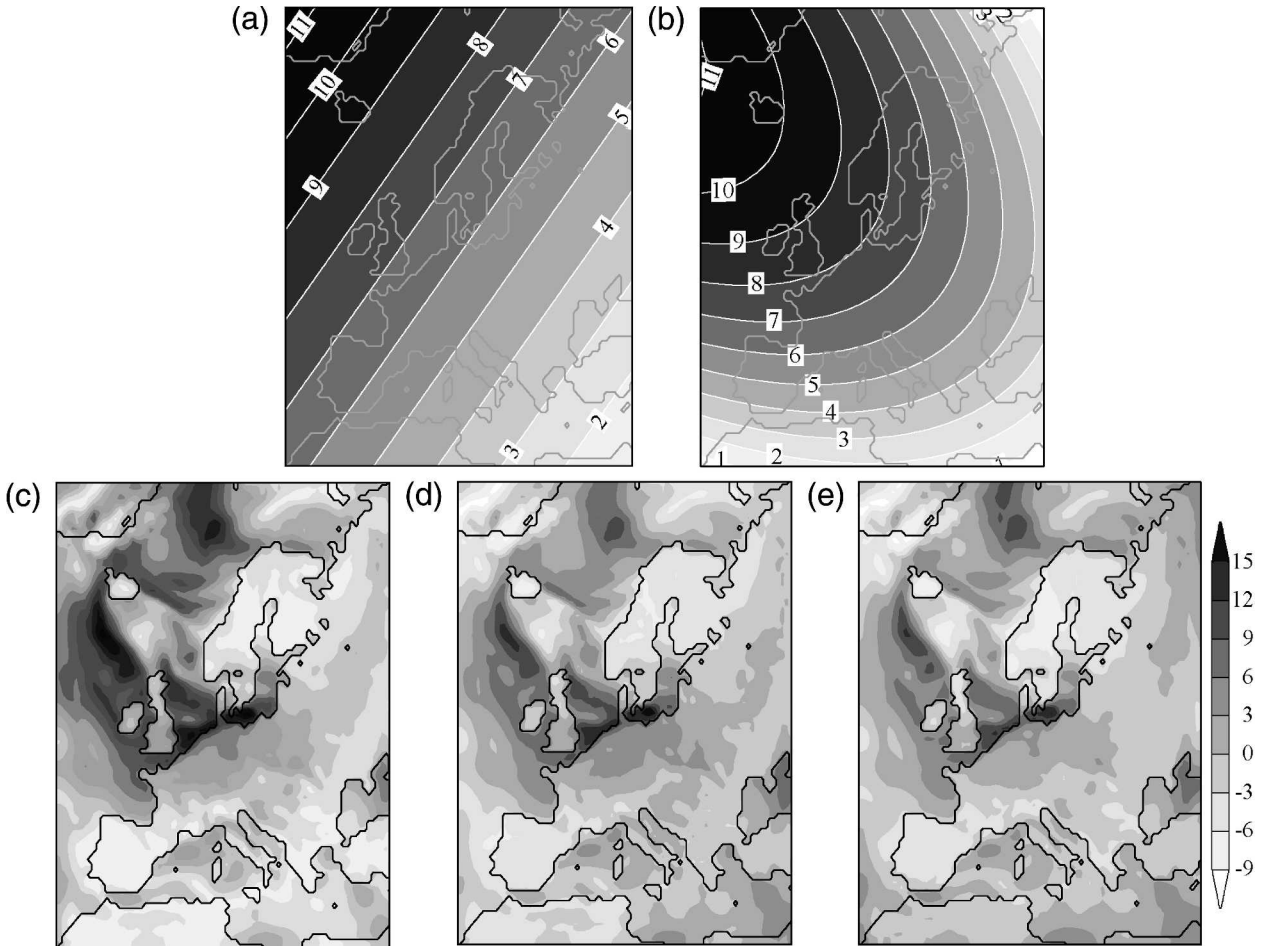

FIG. 2. (top) $K = 1, 2$ polynomials P_u^1 and P_u^2 fitted to the wind speed field (m s^{-1}) at a height of 10 m at 1800 UTC 3 Dec 1999 (storm Anatol). (bottom) Full wind speed field for the same date, and after subtraction of the $K = 1, 2$ polynomials, i.e., $u - P_u^1$ and $u - P_u^2$.

large number—say 20. In the intermediate range, the response is expected to smoothly transform from 1 to 0. It is advisable that the two regions with specified responses are not covering the entire domain; instead a band of unspecified responses should be used in an in-between region.

Similarly, high-pass and bandpass filters can be constructed. For a bandpass filter three parameters have to be selected, a region with zero responses for small and large wavenumbers, and a response of one for medium wavenumbers.

4. Filter weights

The filter array must be quadratic and symmetrical with respect to the zonal and meridional directions, and also with respect to both diagonals. Thus, only a few filter weights are to be determined, in the sketch marked by "x," while those determined by symmetry are given by "o," for instance in a filter with 9 and with 25 weights:

```
          o o o o o
  o o o   o o o o o
  o x o   o o x o o .
  o x x   o o x x o
          o o x x x
```

Apart from the central point, which is weighted by the central filter weight $a_{0,0}$, N points to the left (top) and N points to the right (bottom) are used, such that $2N + 1$ points are considered in either direction. For a LAM domain of 81×91 grid points we chose filters with $N = 8$ points, so that their spatial extension is $(2N + 1) \times (2N + 1) = 17 \times 17$ points.

The symmetric conditions are $a_{m,n} = a_{-m,n} = a_{m,-n} = a_{-m,-n} = a_{n,m}$, whereby subscripts n and m denote rows and columns, respectively. Thus, the filter weights $a_{n,m}$

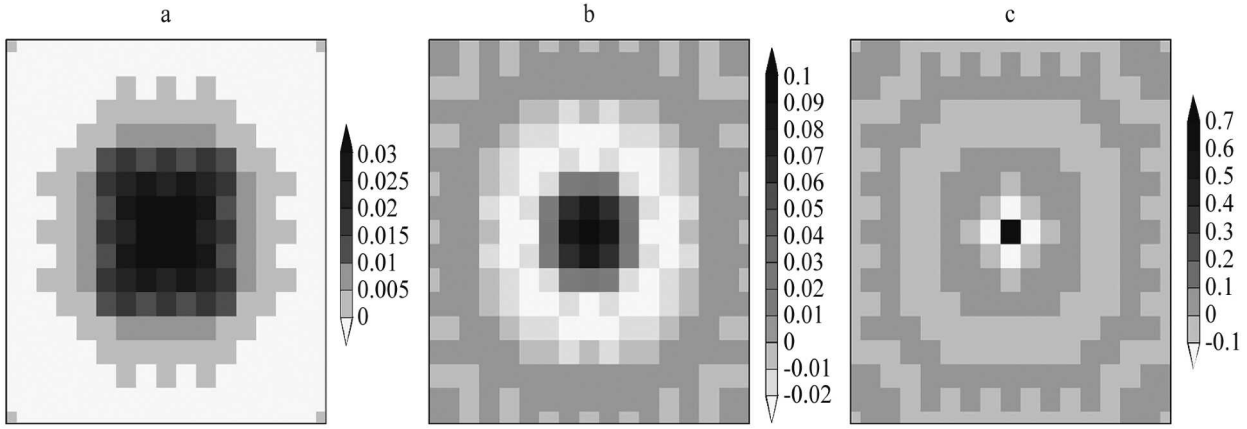

FIG. 3. Filter weights for a (a) low-pass, (b) bandpass, and (c) high-pass filter. Here $a_{0,0}$ is in the center; representation as in Eq. (2). The axes denote grid points of the LAM. Filters were chosen with $N = 8$ points, so that their spatial extension is $(2N + 1) \times (2N + 1) = 17 \times 17$ points.

look like the following in the case of a filter with 25 weights:

$$\begin{pmatrix} a_{-2,-2} & a_{-2,-1} & a_{-2,0} & a_{-2,1} & a_{-2,2} \\ a_{-1,-2} & a_{-1,-1} & a_{-1,0} & a_{-1,1} & a_{-1,2} \\ a_{0,-2} & a_{0,-1} & a_{0,0} & a_{0,1} & a_{0,2} \\ a_{1,-2} & a_{1,-1} & a_{1,0} & a_{1,1} & a_{1,2} \\ a_{2,-2} & a_{2,-1} & a_{2,0} & a_{2,1} & a_{2,2} \end{pmatrix} = \begin{pmatrix} a_{2,2} & a_{2,1} & a_{2,0} & a_{2,1} & a_{2,2} \\ a_{2,1} & a_{1,1} & a_{1,0} & a_{1,1} & a_{2,1} \\ a_{2,0} & a_{1,0} & a_{0,0} & a_{1,0} & a_{2,0} \\ a_{2,1} & a_{1,1} & a_{1,0} & a_{1,1} & a_{2,1} \\ a_{2,2} & a_{2,1} & a_{2,0} & a_{2,1} & a_{2,2} \end{pmatrix}. \quad (2)$$

The resulting filter weights for a low-, band-, and high-pass filter are shown in Fig. 3. The low-pass-filter weights (Fig. 3a) show a homogenous structure with highest values in the middle of the weighting area and decreasing values farther away from the filter base point. This will result in a large mean value and therefore a low-pass-filtered field. The bandpass-filter weights (Fig. 3b) include several transitions between positive and negative values, and thereby the mean value will be filtered and only the smaller structures will remain. This is even more strongly enforced for the high-pass-filter weights (Fig. 3c), which comprise a yet higher number of changes in sign. Thus, only the smallest structures will pass this filter.

5. Response function

We assume a 2D periodical function f that can be expanded into Fourier components:

$$f(x, y) = \sum_{k,l=-K}^{K} \alpha_{kl} e^{i(kx+ly)} \quad (3)$$

with the Fourier coefficients $\alpha_{k,l} = \alpha^*_{-k,-l}$ because $f(x, y)$ is a real function; k and l are the zonal and meridional wavenumbers, respectively. The arguments x and y vary between 0 and 2π. The filtered function $\tilde{f}$ is given by

$$\tilde{f}(x, y) = a_{0,0} f(x, y) + A + B + C \quad (4)$$

with

$$\begin{aligned} A = &\sum_{n=1}^{N} a_{n,0}[f(x, y + \hat{n}) + f(x, y - \hat{n}) + f(x + \hat{n}, y) \\ &+ f(x - \hat{n}, y)], \\ B = &\sum_{n=1}^{N} a_{n,n}[f(x + \hat{n}, y + \hat{n}) + f(x + \hat{n}, y - \hat{n}) \\ &+ f(x - \hat{n}, y + \hat{n}) + f(x - \hat{n}, y - \hat{n})], \\ C = &\sum_{n=2}^{N} \sum_{m=1}^{n-1} a_{n,m}[f(x + \hat{n}, y + \hat{m}) + f(x + \hat{n}, y - \hat{m}) \\ &+ f(x - \hat{n}, y + \hat{m}) + f(x - \hat{n}, y - \hat{m}) \\ &+ f(x + \hat{m}, y + \hat{n}) + f(x + \hat{m}, y - \hat{n}) \\ &+ f(x - \hat{m}, y + \hat{n}) + f(x - \hat{m}, y - \hat{n})], \end{aligned} \quad (5)$$

with the convention $\hat{n} = n \cdot 2\pi/L$ and $\hat{m} = m \cdot 2\pi/L$. Here, L is the number of grid points, which are counted by the integers n and m. The transformation from n to $\hat{n}$ is required, as we have written (3) for functions defined on the interval $[0, 2\pi]$. The filter weights are denoted by $a_{n,m}$, and A represents the central row and column of matrix (2), B the diagonals, and C the re-

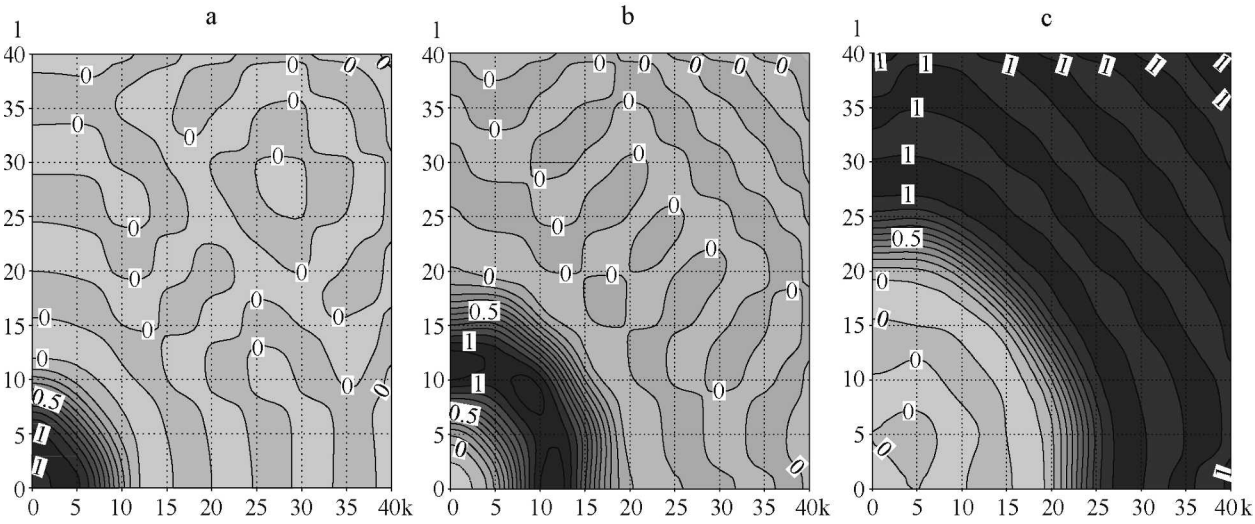

FIG. 4. Response functions for the (a) low-pass, (b) bandpass, and (c) high-pass filters with the filter weights of Fig. 3. The axes show the zonal wavenumbers k (x axis) and the meridional wavenumbers l (y axis).

maining elements. Further detailed calculation steps are given in appendix B.

The filtered function may also be expanded into a Fourier decomposition

$$\tilde{f}(x, y) = \sum_{k,l=-L}^{K} \tilde{\alpha}_{k,l} e^{i(kx+ly)} \tag{6}$$

with $\tilde{\alpha}_{k,l} = \tilde{\alpha}^*_{-k,l} = \tilde{\alpha}^*_{k,-l} = \tilde{\alpha}_{-k,-l}$. The response function is given by

$$\kappa(k, l) = \tilde{\alpha}_{k,l}/\alpha_{k,l}. \tag{7}$$

By concatenating the various contributions in (4), the response function κ can be written as in the following for wavenumbers $k, l = -K, -K + 1 \ldots -1, 0, 1 \ldots K - 1$, K:

$$\begin{aligned}\kappa(k, l) = a_{0,0} &+ \sum_{n=1}^{N} \{2a_{n,0}[\cos(k\hat{n}) + \cos(l\hat{n})] \\ &+ 4a_{n,n}\cos(k\hat{n})\cos(l\hat{n})\} \\ &+ 4\sum_{n=2}^{N}\sum_{m=1}^{n-1} a_{n,m}[\cos(k\hat{n})\cos(l\hat{m}) \\ &+ \cos(l\hat{n})\cos(k\hat{m})].\end{aligned} \tag{8}$$

The constants 2 and 4 in (8) account for the multiple uses of the filter weights in one filtering step. The response functions are shown in Fig. 4 for the (a) low-pass, (b) bandpass, and (c) high-pass filters with the filter weights of Fig. 3. The wavenumber ranges were chosen as in the following for the low-pass filter:

$$\kappa(k^*) = 1 \quad \text{for all} \quad k^* \le 6 \quad \text{and}$$
$$\kappa(k^*) = 0 \quad \text{for all} \quad k^* \ge 11;$$

for the bandpass filter:

$$\kappa(k^*) = 0 \quad \text{for all} \quad k^* \le 6,$$
$$\kappa(k^*) = 1 \quad \text{for all} \quad k^* \ge 8 \quad \text{and} \quad \le 16, \quad \text{and}$$
$$\kappa(k^*) = 0 \quad \text{for all} \quad k^* \ge 18;$$

and for the high-pass filter:

$$\kappa(k^*) = 0 \quad \text{for all} \quad k^* \le 21 \quad \text{and}$$
$$\kappa(k^*) = 1 \quad \text{for all} \quad k^* \ge 26$$

for a filter of 17 × 17 grid points used for an LAM domain of 81 × 91 grid points. The response functions show a well-defined wavenumber range where the response is close to 1 and a smooth transition to response values of about 0. The transition area can be selected quite narrowly as can be seen for the bandpass filter (b), which results in a rather sharply defined filter.

Some cases of overshooting of the response function occurred when the areas of response values of 1 and 0 were chosen in a way that the transition area in between was too narrow, so that only a small number of unspecified responses resulted. Overshooting can be identified by locating large positive or negative values in the response function that are far beyond the values of 0 or 1. In that case the response function showed very irregular patterns compared to the smooth patterns shown in Fig. 4. To prevent overshooting it is advisable that the regions with specified responses are not covering the entire domain and that they are well separated so that there is enough space for unspecified responses.

6. Optimal discrete filters

Equation (8) is linear in the coefficients $a_{0,0}$, $a_{1,0}$, $a_{2,0}$, $a_{2,1} \ldots a_{N,1}$. If the filter has the width $2N + 1$, then $(N + 1) \cdot (N + 2)/2$ coefficients need to be determined. This can be done by specifying responses $\kappa(k, l)$ at a variety of wavenumbers, so that a set of linear equations is obtained:

$$\begin{aligned}\kappa(k, l) = a_{0,0} &+ 2a_{1,0}[\cos(k\hat{1}) + \cos(l\hat{1})] \\ &+ 4a_{1,1}\cos(k\hat{1})\cos(l\hat{1}) \\ &+ 4\sum_{n=1}^{N}\{2a_{n,0}[\cos(k\hat{n}) + \cos(l\hat{n})] \\ &+ \sum_{m=1}^{n-1} a_{n,m}4[\cos(k\hat{n})\cos(l\hat{m}) + \cos(l\hat{n})\cos(k\hat{m})] \\ &+ 4a_{n,n}\cos(k\hat{n})\cos(l\hat{n})\}. \end{aligned} \tag{9}$$

When we introduce the notation $A_1 = a_{0,0}$, $A_2 = a_{1,0}$, $A_3 = a_{1,1}$, and

$$A_{n\cdot(n+1)/2+1+m} = a_{n,m} \quad \text{for} \quad n \geq 2 \quad \text{and} \quad m = 0 \ldots n \tag{10}$$

and

$$\begin{aligned} M_{K,1} &= 1 \\ M_{K,n\cdot(n+1)/2+1} &= 2[\cos(k\hat{n}) + \cos(l\hat{n})] \quad \text{for } n \geq 1 \\ M_{K,n\cdot(n+1)/2+1+m} &= 4[\cos(k\hat{n})\cos(l\hat{m}) \\ &\quad + \cos(l\hat{n})\cos(k\hat{m})] \\ &\text{for} \quad m = 1 \ldots n - 1 \quad \text{and} \quad n \geq 2 \\ M_{K,n\cdot(n+1)/2+1+n} &= 4\cos(k\hat{n})\cos(l\hat{n}) \quad \text{for} \quad n \geq 1. \end{aligned} \tag{11}$$

Equation (9) may be rewritten with $K = (k, l)$:

$$\kappa(K) = \sum_{j=1}^{(N+1)\cdot(N+2)/2} M_{K,j}A_j. \tag{12}$$

One option is to select as many wavenumbers with specified responses as the number of weights $(N + 1) \cdot (N + 2)/2$. In that case, a linear set of equations with an invertible matrix emerges. We have tried this out, but unsatisfactory results emerged—the solution for the two-dimensional response function κ is a superposition of waves, and fixing κ at a number of selected wavenumbers creates a two-dimensional κ that fits exactly the specified responses at a few locations, but between these locations unacceptable overshooting phenomena emerged, in particular when band- and high-pass filters were constructed.

Therefore, the response is specified at more wavenumbers than there are filter weights. Then, the set of linear equations is overdetermined. An approximate solution is obtained by minimizing

$$\sum_K \left(\kappa(K) - \sum_{j=1}^{(N+1)\cdot(N+2)/2} M_{K,j}A_j\right)^2. \tag{13}$$

The filter weights solution for this problem is given by

$$\mathrm{A} = (\mathbf{M}^{\mathrm{T}}\mathbf{M})^{-1}\mathbf{M}^{\mathrm{T}}\boldsymbol{\kappa} \tag{14}$$

with the matrix $\mathbf{M}$ with $(N + 1) \cdot (N + 2)/2$ columns (dimension of $\mathbf{A}$) and as many rows as wavenumbers have been selected with given responses (dimension of $\boldsymbol{\kappa}$). Please note that the sum of the filtered plus the polynomial pieces does not equal the total. The individual filtered pieces are not orthogonal to each other. That is, the variances of the different contributions do not add exactly to the total variance. This would be a nice property to have, but for the specific purpose in mind, namely the characterization of phenomena on different scales, this is not really needed.

7. Applications

The results of a regional model run (Feser et al. 2001) for western Europe forced with the NCEP reanalyses (Kalnay et al. 1996) were filtered with the presented filter for three wavenumber ranges. The quadratic polynomials (section 2) were subtracted before applying the band- and high-pass filters. A first example for the storm "Anatol" can be seen in Fig. 5. It shows the (a) unfiltered, (b) low-pass-, (c) bandpass-, and (d) high-pass-filtered wind speed fields at a height of 10 m for 1800 UTC 3 December 1999 for western Europe when the storm was centered over the northeastern tip of Denmark with a low pressure core of 956 hPa. The low-pass-filtered field (b) shows the smoothed field and displays only the very large scales. The bandpass-filtered data (c) lack the large-scale information and show land–sea interactions on the regional scale but also regional wind speed structures over the North Sea connected with the intense low pressure system. The high-pass-filtered part (d) displays the smallest scales with largest values almost exclusively in the coastal zones for this wind speed example. An effective scale separation was achieved.

The bandpass- and high-pass-filtered fields show anomalies from the large-scale field; therefore the val-

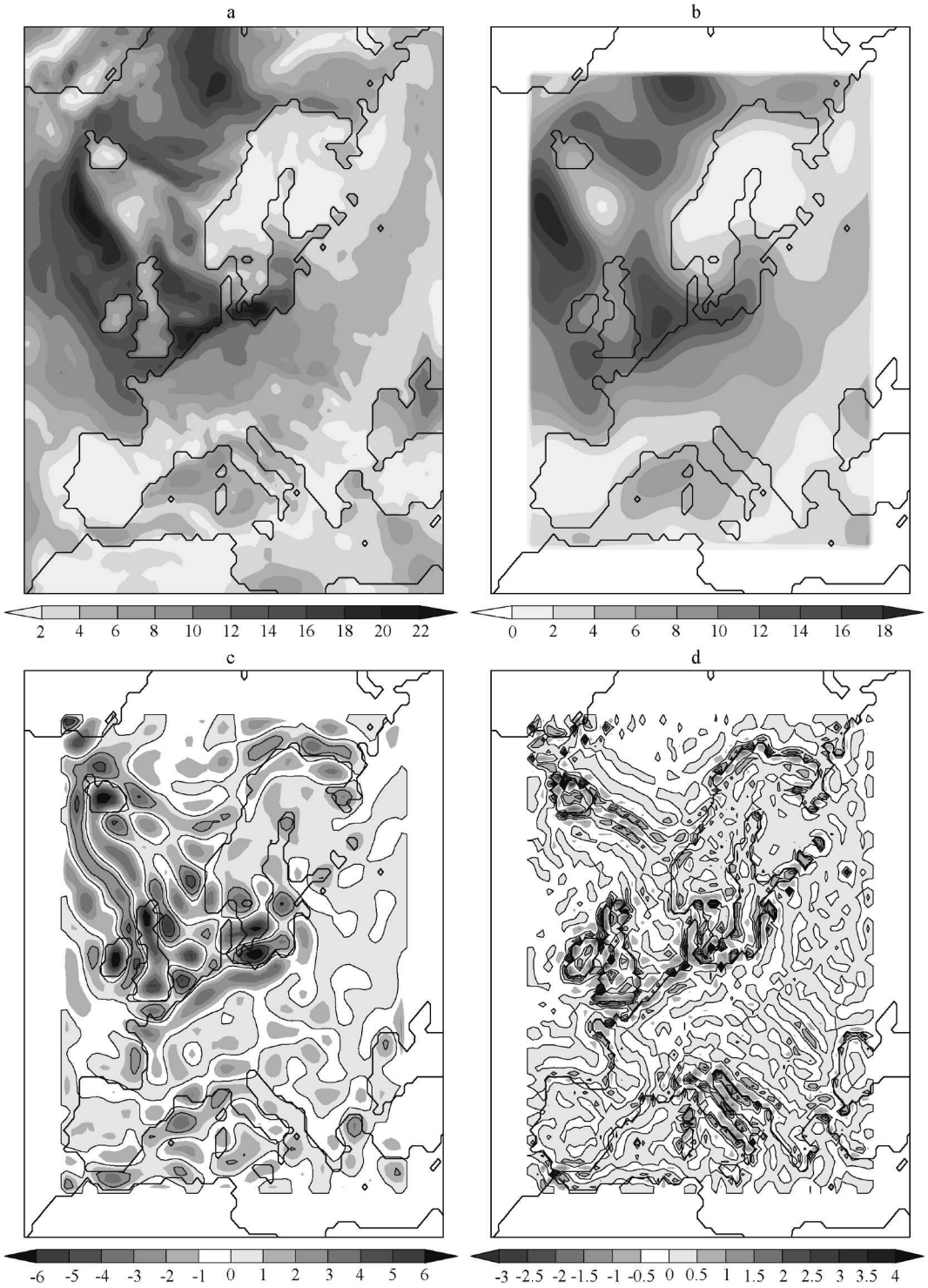

FIG. 5. The 10-m wind speed fields (m s^{-1}) for the storm Anatol at 1800 UTC 3 Dec 1999 of a LAM simulation: (a) unfiltered, (b) low-pass-filtered, (c) bandpass-filtered, and (d) high-pass-filtered data. For (c) and (d) the positive anomalies are also shown as contour lines so that they can be distinguished from the negative anomalies.

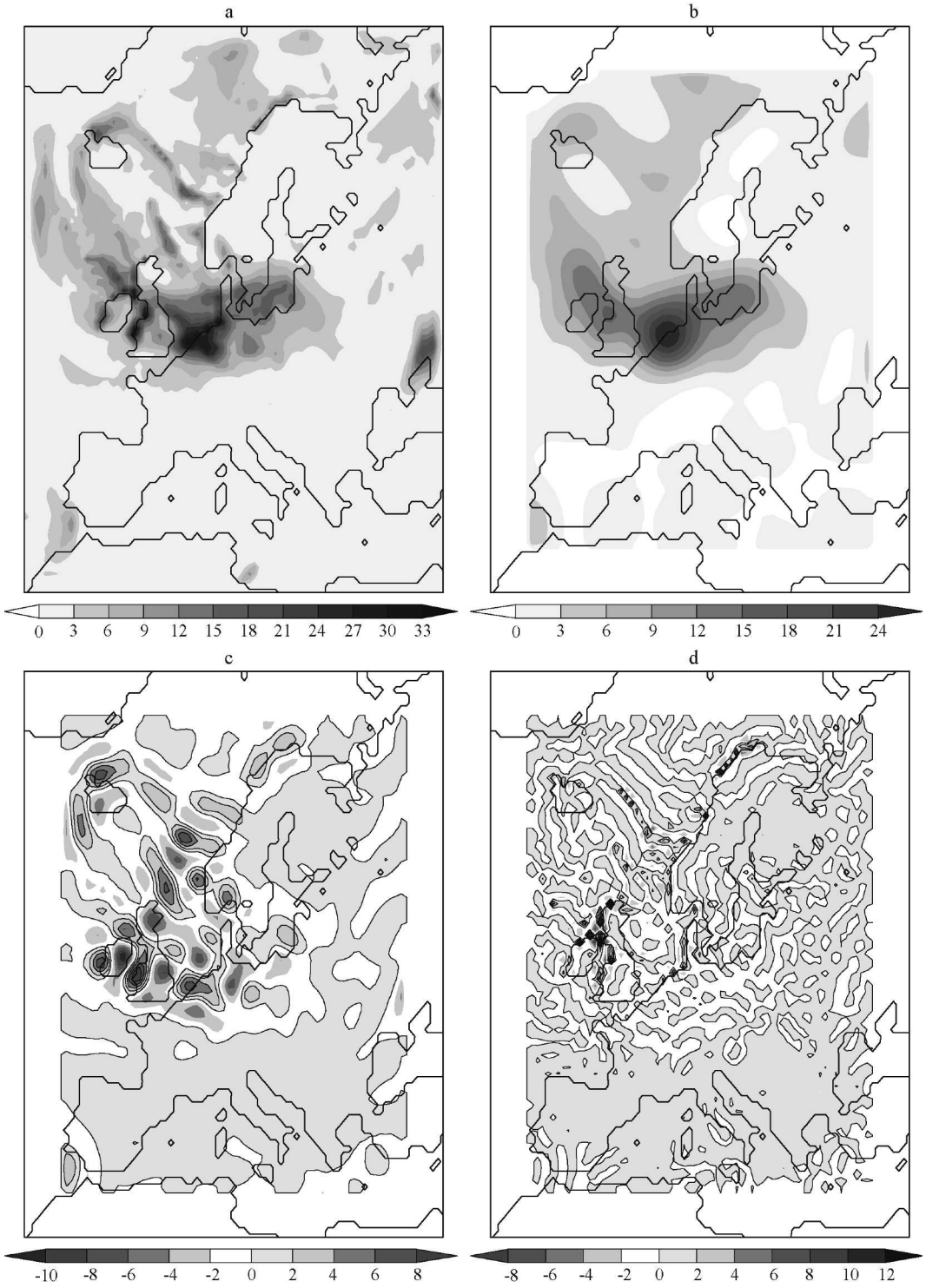

FIG. 6. Precipitation fields (mm) for the storm Anatol accumulated for 1800 UTC 3 Dec 1999 of a LAM simulation: (a) unfiltered, (b) low-pass-filtered, (c) bandpass-filtered, and (d) high-pass-filtered data. For (c) and (d) the positive anomalies are also shown as contour lines so that they can be distinguished from the negative anomalies.

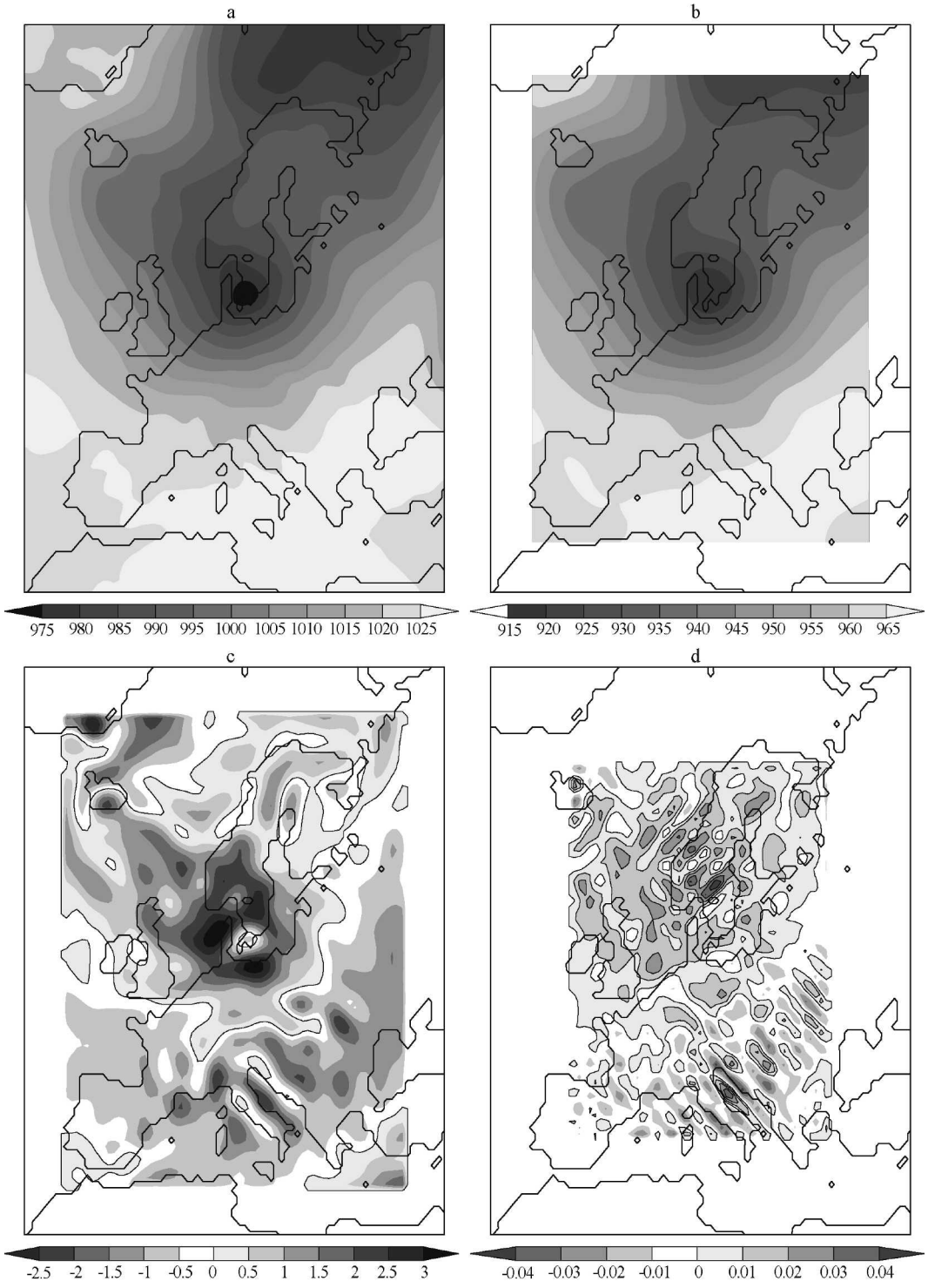

FIG. 7. Mean sea level pressure (hPa) for the storm Anatol at 1800 UTC 3 Dec 1999 of a LAM simulation: (a) unfiltered, (b) low-pass-filtered, (c) bandpass-filtered, and (d) high-pass-filtered data. For (c) and (d) the positive anomalies are also shown as contour lines so that they can be distinguished from the negative anomalies. Note that the low-pass-filtered field is reduced in the overall level, which reflects the fact that the filter only approximately conserves the spatial mean.

ues are positive and negative around the zero point. The white "frames" around the filtered fields are a result of the digital filter's weighted average operation around a base point, which cannot be calculated in the direct vicinity of the LAM's boundaries due to a lack of grid points. Therefore the points close to the lateral boundaries (in our example eight rows and columns of grid points, which is equal to the sponge zone width of the LAM we used) have a value of zero.

Another example of the filter application is given in Fig. 6. It shows precipitation fields for the storm Anatol, accumulated for 3 December 1999. Again, the (a) unfiltered, (b) low-pass-, (c) bandpass-, and (d) high-pass-filtered fields are shown. The low-pass- and the bandpass-filtered data display the frontal precipitation related to the intense low pressure system on their respective scale. Also the high-pass-filtered precipitation is most intense in the vicinity of the storm's cloud systems.

Figure 7 shows the mean sea level pressure field for the storm Anatol. The storm center over the northeastern tip of Denmark can be seen both in the unfiltered and low-pass-filtered fields [(a) and (b)]. The bandpass-filtered data (c) depict anomalies around the low pressure core and over the North Atlantic. For calculating the high-pass-filtered field (d) not only were the polynomials subtracted, but also the low-pass-filtered field (whereby the polynomials were subtracted as well). This was necessary because the spectrum of the mean sea level field drops off rather sharply so that the remnants of large-scale features in the high-pass-filtered field S_f are comparable to the small-scale features. Therefore, the large-scale contribution is suppressed explicitly before high-pass filtering by calculating $f - P_f^K - L_{f-P_f^K}$. Then, this reduced field is filtered. Because of the double-filter application, the spatial extension of the data is decreased; now there are 16 instead of 8 rows and columns of zero value around the filtered data. The largest anomalies can be seen north of the low pressure core and over the North Sea.

Since the main purpose of this paper is to present the method of spatial two-dimensional discrete filtering and not the application of it we will not go into further detail here. For further studies the filter may be used as a tool to compare such fields for model evaluation, for process studies on different spatial scales, or to show the resolvable scales of the LAM.

8. Summary and conclusions

In this paper we have presented a method to construct isotropic digital filters suited for scale separations of atmospheric fields on limited-area grids. There are several methods to do scale separations; like Fourier filtering, the discrete cosine transform, or digital filters. We suggest using near-isotropic two-dimensional digital filters because these filters operate with a finite basis, can be constructed flexibly, and are easily implemented and run with little computation cost. Our method allows the construction of filters for a broad range of applications and for data on homogeneous, limited-area grids. A wavenumber range of interest has to be selected and the best-fitting response values can then be calculated automatically using an approximation method. The filter weights are then calculated by a matrix inversion.

In our example, we constructed several isotropic discrete filters for differing wavenumber ranges, to isolate the large, medium, and small scales of limited-area atmospheric fields. Applications of the filters produced reasonable results.

As a next step we will apply these filters for model evaluation purposes, to study processes on a limited-area domain or to advance with the question of added value of regional models.

Acknowledgments. We are grateful to R. Laprise for valuable discussions regarding this work. He proposed the idea of a full two-dimensional filter. We thank M. Quante for the discussion on wavelet analyses, and M. Widmann and R. Weisse for reading the manuscript and for their constructive modification proposals. We thank B. Gardeike who prepared some of the figures for us.

APPENDIX A

Polynomial Fit

a. Formal presentation of problem

We want to expand a discrete set of numbers x_{ij} on a rectangular grid of points (i, j) with $i = 1 \ldots n_x$ and $j = 1 \ldots n_y$ into a polynomial of order K, that is,

$$x_{i,j} = \sum_{r,q=0}^{r+q \le K} a_{r,q} i^r j^q + \varepsilon_{i,j}, \tag{A1}$$

where a values are the polynomial coefficients that are to be determined, and r and q are the indices that number serially the polynomial terms. Here, ε represents a remainder, and the square of sums $\Sigma_{i,j}\, \varepsilon_{i,j}^2$ is assumed to be minimum. The sum is made up of $(K + 1)\,(K + 2)/2$ terms.

This expression (A1) means for

$$\begin{aligned} K = 0: \quad & x_{i,j} = a_{0,0} + \varepsilon_{i,j} \\ K = 1: \quad & = a_{0,0} + a_{1,0} i + a_{0,1} j + \varepsilon_{i,j} \\ K = 2: \quad & = a_{0,0} + a_{1,0} i + a_{2,0} i^2 + a_{0,1} j + a_{0,2} j^2 \\ & \quad + a_{1,1} i, j + \varepsilon_{i,j} \end{aligned}$$

etc.

The expansion (A1) may be rewritten as

$$x_{i,j} = \sum_{k=0}^{K} T_k + \varepsilon_{i,j}, \tag{A2}$$

with

$$T_k = \sum_{q=0}^{K-k} a_{k,q} i^k j^q. \tag{A3}$$

For example:

$$\begin{aligned} K = 1: \quad & T_0 = a_{0,0} + a_{0,1} j \\ & T_1 = a_{1,0} i \\ K = 2: \quad & T_0 = a_{0,0} + a_{0,1} j + a_{0,2} j^2 \\ & T_1 = a_{1,0} i + a_{1,1} ij \\ & T_2 = a_{2,0} i^2. \end{aligned}$$

For a given field $x_{i,j}$, we want to determine optimal coefficients $a_{r,q}$ so that

$$\hat{\varepsilon} = \sum_{i,j} \left[x_{i,j} - \sum_{k=0}^{K} T_k \right]^2 = \min. \tag{A4}$$

b. Solution of minimum problem

The minimum of (A4) is derived by first calculating derivatives with respect to the quantity to be determined, and then finding zeros of these derivatives, that is,

$$\frac{\partial \hat{\varepsilon}}{\partial a_{r,q}} = 0. \tag{A5}$$

It is $(\partial \Sigma T_k / \partial a_{r,q}) = (\partial T_r / \partial a_{r,q}) = i^r j^q$, and thus

$$\begin{aligned} \frac{\partial \hat{\varepsilon}}{\partial a_{r,q}} &= \sum_{i,j} \left[\frac{\partial}{\partial a_{r,q}} (x_{i,j} - \sum_{k=0}^{K} T_k)^2 \right] \\ &= \sum_{i,j} \left[2(x_{i,j} - \sum_{k=0}^{K} T_k) \left(- \frac{\partial T_r}{\partial a_{r,q}} \right) \right] \\ &= 2 \sum_{i,j} \sum_{k=0}^{K} T_k i^r j^q - 2 \sum_{i,j} x_{i,j} i^r j^q \end{aligned}$$

or for all pairs (r, q):

$$\sum_{k=0}^{K} \sum_{s=0}^{K-k} a_{k,s} \sum_{i,j} (i^k j^s)(i^r j^q) = \sum_{i,j} x_{i,j} i^r j^q. \tag{A6}$$

Setting this derivative to zero results in a set of linear equations for all $(K + 1)(K + 2)/2$ coefficients $a_{r,q}$. Thus, the problem is reduced to a conventional matrix inversion problem. A minor technical challenge is to properly map the two-dimensional index (r, s) on a one-dimensional index.

APPENDIX B

Response Function of 2D Digital Filter

To determine the response function κ of the filter, (3) is inserted in (4). Because of $e^{ix} + e^{-ix} = 2\cos(x)$, the terms A, B, and C can be rewritten as

$$\begin{aligned} A &= \sum_{n=1}^{N} a_{n,0} \left[\sum_{k,l=-K}^{K} \alpha_{k,l} e^{i(kx+ly)} (e^{ik\hat{n}} + e^{-ik\hat{n}} + e^{il\hat{n}} + e^{-il\hat{n}}) \right] \\ &= 2 \sum_{n=1}^{N} a_{n,0} \left\{ \sum_{k,l=-K}^{K} \alpha_{k,l} e^{i(kx+ly)} [\cos(k\hat{n}) + \cos(l\hat{n})] \right\} \\ &= \sum_{k,l=-K}^{K} \left\{ 2 \sum_{n=1}^{N} a_{n,0} [\cos(k\hat{n}) + \cos(l\hat{n})] \right\} \alpha_{k,l} e^{i(kx+ly)}, \end{aligned}$$

$$\begin{aligned} B &= \sum_{n=1}^{N} a_{n,n} \left[\sum_{k,l=-K}^{K} \alpha_{k,l} e^{i(kx+ly)} (e^{ik\hat{n}+il\hat{n}} + e^{-ik\hat{n}-il\hat{n}} + e^{ik\hat{n}-il\hat{n}} + e^{-ik\hat{n}+il\hat{n}}) \right] \\ &= \sum_{n=1}^{N} a_{n,m} \left\{ \sum_{k,l=-K}^{K} \alpha_{k,l} e^{i(kx+ly)} 2[e^{ik\hat{n}} \cos(l\hat{n}) + e^{-ik\hat{n}} \cos(ln)] \right\} \\ &= \sum_{k,l=-K}^{K} \left[4 \sum_{n=1}^{N} a_{n,n} \cos(kn) \cos(ln) \right] \alpha_{k,l} e^{i(kx+ly)}, \end{aligned}$$

and

$$
\begin{aligned}
C &= \sum_{n=2}^{N}\sum_{m=1}^{n-1} a_{n,m} \sum_{k,l=-K}^{K} \alpha_{k,l} e^{i(kx+ly)}[e^{ik\hat{n}+il\hat{m}} + e^{ik\hat{n}-il\hat{m}} + e^{-ik\hat{n}+il\hat{m}} + e^{-ik\hat{n}-il\hat{m}} + e^{ik\hat{m}+il\hat{n}} \\
&\quad + e^{ik\hat{m}-il\hat{n}} + e^{-ik\hat{m}+il\hat{n}} + e^{-ik\hat{m}-il\hat{n}}] \\
&= \sum_{n=2}^{N}\sum_{m=1}^{n-1} a_{n,m} \sum_{k,l=-K}^{K} \alpha_{k,l} e^{i(kx+ly)} 2[e^{ik\hat{n}} \cos(l\hat{m}) + e^{-ik\hat{n}} \cos(l\hat{m}) + e^{ik\hat{m}} \cos(l\hat{n}) + e^{-ik\hat{m}} \cos(l\hat{n})] \\
&= \sum_{k,l=-K}^{K} \left\{ 4 \sum_{n=2}^{N}\sum_{m=1}^{n-1} a_{n,m}[\cos(k\hat{n}) \cos(l\hat{m}) + \cos(l\hat{n}) \cos(k\hat{m})] \right\} \alpha_{k,l} e^{i(kx+ly)}.
\end{aligned}
$$

REFERENCES

Bettge, T. W., and D. P. Baumhefner, 1980: A method to decompose the spatial characteristics of meteorological variables within a limited domain. *Mon. Wea. Rev.,* **108,** 843–854.

Daubechies, I., 1992: *Ten Lectures on Wavelets*. CBMS-NFS Regional Conference Series in Applied Mathematics, Vol. 61, SIAM, 357 pp.

Denis, B., J. Côté, and R. Laprise, 2002: Spectral decomposition of two-dimensional atmospheric fields on limited-area domains using the discrete cosine transform (DCT). *Mon. Wea. Rev.,* **130,** 1812–1829.

Desrochers, P. R., and S. Y. K. Yee, 1999: Wavelet applications for mesocyclone identification in Doppler radar observations. *J. Appl. Meteor.,* **38,** 965–980.

Errico, R., 1985: Spectra computed from a limited area grid. *Mon. Wea. Rev.,* **113,** 1554–1562.

——, 1987: A comparison between two limited-area spectral analysis schemes. *Mon. Wea. Rev.,* **115,** 2856–2861.

Feser, F., R. Weisse, and H. von Storch, 2001: Multi-decadal atmospheric modeling for Europe yields multi-purpose data. *Eos, Trans. Amer. Geophys. Union,* **82,** 305–310.

Giorgi, F., and Coauthors, 2001: Regional climate information—Evaluation and projections. *Climate Change 2001: The Scientific Basis,* J. T. Houghton et al., Cambridge University Press, 583–638.

Jameson, L., T. Waseda, and H. Mitsudera, 2002: Scale utilization and optimization from wavelet analysis for data assimilation: SUgOiWADAi. *J. Atmos. Oceanic Technol.,* **19,** 747–758.

Kalnay, E., and Coauthors, 1996: The NCEP/NCAR 40-Yr Reanalysis Project. *Bull. Amer. Meteor. Soc.,* **77,** 437–471.

Mallat, S., 1989: A theory for multiresolution signal decomposition: The wavelet representation. *IEEE Trans. Patt. Recog., Mach. Intell.,* **11,** 674–693.

——, 1998: *A Wavelet Tour of Signal Processing.* Academic Press, 577 pp.

Miguez-Macho, G., G. L. Stenchikov, and A. Robock, 2004: Spectral nudging to eliminate the effects of domain position and geometry in regional climate model simulations. *J. Geophys. Res.,* **109,** D13104, doi:10.1029/2003JD004495.

Raymond, W. H., 1989: High-order, high-pass implicit filters for evaluating information within finite areas. *Mon. Wea. Rev.,* **117,** 2772–2781.

Shapiro, R., 1970: Smoothing, filtering, and boundary effects. *Rev. Geophys. Space Phys.,* **8,** 359–387.

——, 1975: Linear filtering. *Math. Comput.,* **29,** 1094–1097.

Shuman, F. G., 1957: Numerical methods in weather prediction: II. Smoothing and filtering. *Mon. Wea. Rev.,* **85,** 357–361.

Stamus, P., F. Carr, and D. Baumhefner, 1992: Application of a scale-separation verification technique to regional forecast models. *Mon. Wea. Rev.,* **120,** 149–163.

Starck, J.-L., F. Murtagh, and A. Bijaoui, 1998: *Image Processing and Data Analysis: The Multiscale Approach.* Cambridge University Press, 287 pp.

von Storch, H., 1995: Inconsistencies at the interface of climate impact studies and global climate research. *Meteor. Z.,* **4,** 72–80.

——, H. Langenberg, and F. Feser, 2000: A spectral nudging technique for dynamical downscaling purposes. *Mon. Wea. Rev.,* **128,** 3664–3673.

Waldron, K. M., J. Paegle, and J. D. Horel, 1996: Sensitivity of a spectrally filtered and nudged limited-area model to outer model options. *Mon. Wea. Rev.,* **124,** 529–547.

Yano, J.-I., M. W. Moncrieff, and X. Wu, 2001: Wavelet analysis of simulated tropical convective cloud systems. Part II: Decomposition of convective-scale and mesoscale structure. *J. Atmos. Sci.,* **58,** 868–876.